Numerical simulation of a low speed fan blade

By Stéphane Moreau †
G. Iaccarino, S. Kang, Y. Khalighi AND M. Wang

The feasibility of using various unsteady turbulence models for the prediction of the wall pressure fluctuations or self-noise sources on a Controlled Diffusion airfoil is evaluated. The aim is to find a possible alternative to a classical body-fitted Large Eddy Simulation for a complex automotive engine cooling fan blade. These unsteady simulations have been compared to wall pressure and wake velocity profiles measured in the large anechoic chamber of Ecole Centrale de Lyon, and to a reference body-fitted Large Eddy Simulation using the dynamic subgrid scale model previously achieved at CTR.

1. Introduction

Broadband self noise or trailing edge noise is due to the scattering of boundary layer vortical disturbances into acoustic waves at the trailing edge of a fan blade. As the only noise contribution in a homogeneous stationary flow, it is a matter of primary interest when addressing the problem of the noise generated by fans (Sharland 1964; Wright 1976; Fukano, Kodama & Senoo 1977; Caro & Moreau 2000), wind turbines (Glegg, Baxter & Glendinning 1987; Hubbard & Shepherd 1991; Parchen *et al.* 1999) and high-lift devices (Pérennès & Roger 1998; Singer, Lockard & Brentner 2000). Self-noise can be reduced if its origin and leading parameters are clearly identified, in terms of flow variables that can be modified through a proper blade design. The prediction of the corresponding broadband noise sources is therefore the prime goal of this study. A first step towards this goal is to study the noise sources of a Controlled-Diffusion (CD) airfoil specifically developed for low Reynolds number automotive engine cooling applications by Valeo. The corresponding set of experiments run in the anechoic wind tunnels of Ecole Centrale Lyon provide the reference aeroacoustic experimental database (Moreau *et al.* 2003; Roger & Moreau 2004).

A first large-eddy simulation (LES) of the flow over the Valeo CD profile (Wang *et al.* 2004) showed that a high quality and fine grid was necessary to achieve numerical stability and yield comparable wall pressure statistics to those obtained experimentally. The sensitivity of the body-fitted single block structured mesh approach to the grid quality and the large computational cost of this airfoil simulation preclude its extension to a realistic automotive engine cooling fan. The latter involves a complex blade geometry with a large variation of blade twist (stagger angle) and rapidly varying blade sweep and rake (highly bowed blades), which makes it hard to reach a high quality single block structured grid over the entire blade span. Moreover the tip clearance involves a much more complex labyrinth than the one considered by You *et al.* (2004), making a local structured body-fitted grid hard to design. Therefore to reach the goal of accurate predictions of wall pressure fluctuations for low speed fan blades, alternative methods need to be explored. The present study will test several numerical approaches as potential

† Valeo Motors and Actuators, France

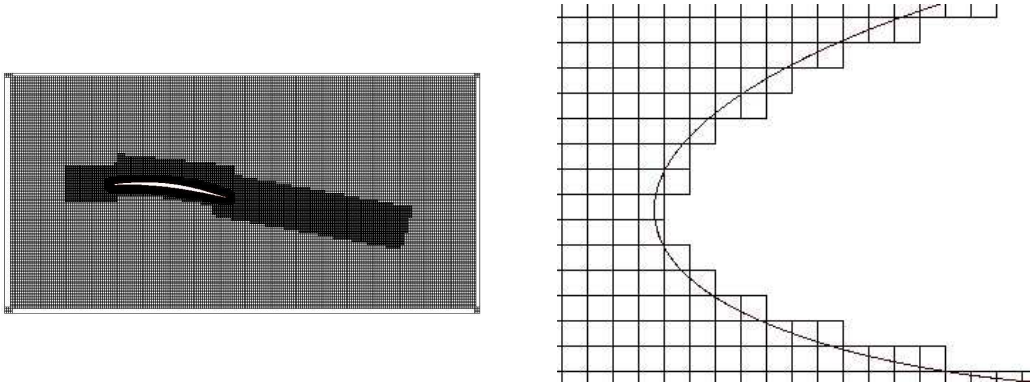

FIGURE 1. Left: Full grid around the CD airfoil used for the Lattice Boltzmann method. Right: Close-up at the leading edge.

alternatives. The Valeo CD airfoil is again considered and the body-fitted LES results serve as reference numerical data.

One way to circumvent the inherent topological difficulties associated with a body-fitted grid for a complex fan blade is to resort to non-boundary conforming methods. Two such promising methods have emerged recently for aerodynamic predictions. The Lattice Boltzmann method (LBM) relies on a pseudo-particle approach and is based on microscopic models and mesoscopic kinetic equations that describe the interaction between the pseudo-particles (Chen & Doolen 1998). The incompressible Navier-Stokes equations are recovered by taking a multi-scale expansion (Chapman-Enskog) of the velocity moments of the particle distribution functions, in the limit of small Knudsen and Mach numbers. On the other hand, the Immersed Boundary method still relies on the direct discretization of the Navier Stokes equations but imposes the boundary conditions indirectly through an additional source term or forcing function added to the flow equations (Mittal & Iaccarino 2005). Both methods employ an "easy-to-generate" non-body conforming Cartesian grid and have a low per-grid-point operation count and massively parallelized algorithms that should lead to fast turn-around simulations. Finally, assuming that the low frequency part of the spectrum is due to the largest vortical structures mainly found in the outer zone of the boundary layer, a Detached Eddy Simulation on a body-fitted grid might also provide an interesting alternative to the more computationally intensive Large Eddy Simulation. This will be the third method tested here. These three methods are first outlined in the next section, with some details on the associated grid and simulation parameters for the CD airfoil. The results are then presented for a Reynolds number based on the chord length of 1.5×10^5 corresponding to the ECL experimental data and the associated reference LES. This transitional Reynolds number represents a real challenge for both Cartesian methods.

2. Numerical approaches

2.1. *Lattice Boltzmann method*

The LBM originates from lattice gas (LG) automata, e.g. a simplified, fictitious and discrete particle kinetics on a discrete lattice with a discrete time. Whereas LG method describes the evolution of a set of Boolean variables, e.g. integers, that represent the particle occupation at the lattice nodes, the LBM method solves for the particle distribution

functions f_i at the lattice nodes i. These real functions are the solutions of the following discrete kinetic equations:

$$f_i\left(\mathbf{x}+\mathbf{e}_i\,\Delta t, t+\Delta t\right) = f_i\left(\mathbf{x},t\right) + \Omega_i\left(f\left(\mathbf{x},t\right)\right) \tag{2.1}$$

where $\mathbf{e}_i$ are the local particle velocities and $\Omega_i\left(f\left(\mathbf{x},t\right)\right)$ is the collision operator which represents the rate of change of f_i resulting from collisions. The macroscopic properties of the fluid are moments of the distribution functions f_i:

$$\rho = \sum_i f_i \qquad\qquad \rho\,\mathbf{u} = \sum_i f_i\,\mathbf{e}_i \tag{2.2}$$

If the local particle distribution is further assumed to relax to an equilibrium state at a single rate τ, the collision operator in equation (2.1) reduces to the lattice Bhatnagar-Gross-Krook (BGK) collision term:

$$\Omega_i\left(f\left(\mathbf{x},t\right)\right) = -\frac{f_i - f_i^{eq}}{\tau} \tag{2.3}$$

In the low Knudsen limit, the rate τ is much smaller than the shortest hydrodynamic time scale and the LBM reproduces the direct simulation of the Navier-Stokes equations (LB-DNS mode). For high Reynolds number, the shortest hydrodynamic time scale or Kolmogorov scale becomes prohibitively small and the rate τ can be replaced by an effective turbulent relaxation time $\tau_{turb} = \tau_0 + C_\mu \frac{k^2}{\epsilon\, T\sqrt{(1+\eta^2)}}$, where τ_0 is the bare molecular relaxation time, T the absolute temperature, $\eta = \frac{S\,k}{\epsilon}$, k the specific turbulent kinetic energy, ϵ the specific dissipation rate, C_μ and S model constants. It can then be shown that the resulting model is similar to a k-ϵ RNG model (LB-RANS model, see Chen *et al.* 2003). All present simulations have been obtained with the commercial code Powerflow from EXA Corporation; the method used (namely Digital Physics) is an extension of the above LBM (Chen, Teixeira & Molvig 1997).

The grid topology around the CD profile, shown in Figure 2 (left), is a rectangular box of similar size as the reference LES grid. The boundary conditions on the box, as in the LES simulation, involve the velocity components on three sides extracted from the RANS simulation of the full ECL test rig and a constant pressure at the outlet. The resulting cartesian grid has 73551 voxels and 1491 surfels in a two-dimensional slice. It involves five levels of consecutive grid refinements. The smallest cell at the leading edge, shown in Figure 2 (right), is five times larger than that in the body-fitted LES grid. The corresponding three-dimensional grid has 3.64 millions voxels and 1.12 million surfels. To improve the resolution at the leading and trailing edges, it includes eight levels of grid refinements (Figure 5c). The highest resolution achieved has 5120 grid points along the chord length. Yet the grid spanwise extension has been limited to 5% of the chord length because of the restriction of the current LBM to cubic voxels.

2.2. *LES with immersed boundary method*

Mittal & Iaccarino (2005) classified several implementations of the immersed boundary method. The present approach belongs to the discrete forcing approach with direct boundary condition imposition. The interpolation scheme is an extension of the interpolation scheme of Fadlun *et al.* (2000). The velocity components at the first grid point off the immersed boundary (IB) are obtained either by using the discretized Navier-Stokes equation or by linear interpolation as in Fadlun *et al.* (2000). A modified version of the latter is used here.

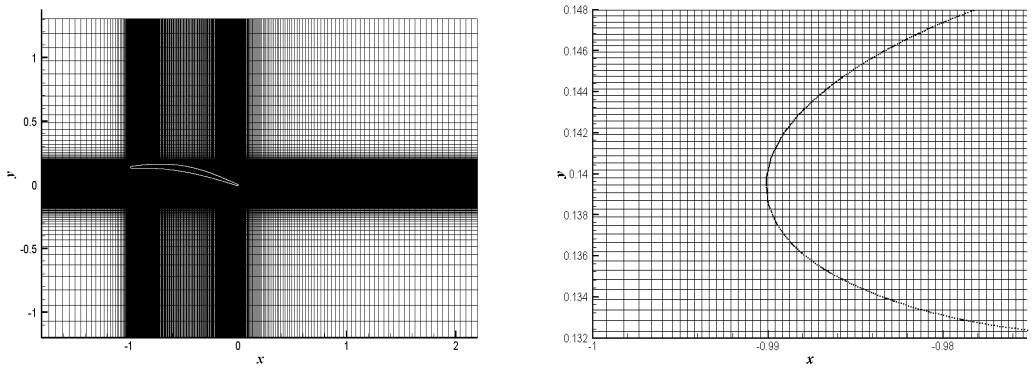

FIGURE 2. Left: Full grid around the CD airfoil used for the immersed boundary method. Right: Close-up at the leading edge.

The interpolation scheme can be written as:

$$\begin{aligned}\hat{u}^k_{i,c} &= w_{i,1}\hat{u}^k_{i,1} + w_{i,2}\hat{u}^k_{i,2} + w_{i,IB}\hat{u}^k_{i,IB} \\ &+ \psi\left(u^{k-1}_i - w_{i,1}u^{k-1}_{i,1} - w_{i,2}u^{k-1}_{i,2} - w_{i,IB}u^{k-1}_{i,IB}\right) \\ &- (\gamma_k+\rho_k)\Delta t\left(\frac{\partial p^{k-1}}{\partial x_i}\,|_c - w_{i,1}\frac{\partial p^{k-1}}{\partial x_i}\,|_1 - w_{i,2}\frac{\partial p^{k-1}}{\partial x_i}\,|_2 - w_{i,IB}\frac{\partial p^{k-1}}{\partial x_i}\,|_{IB}\right),\end{aligned} \tag{2.4}$$

where the subscripts 1 and 2 denote adjacent velocity nodes in the x_1 and x_2 directions, and subscript IB denotes the point on the IB which is the boundary-normal projection of the velocity node c, and w_i is an interpolation coefficient determined by the geometric configuration. Δt is the time step, k is the sub-step index, γ_k and ρ_k are coefficients used in the third order Runge-Kutta scheme, and $\psi = \sqrt{(w_{i,1}+w_{i,2})/w_{i,IB}}$ $(\psi \leq 1)$. Note that if the last two terms in equation (2.4) are omitted the standard linear interpolation formula is recovered. The present approach is based on the fractional step method (Kim & Moin 1985) with Crank-Nicolson scheme for the diffusion terms and the third-order Runge-Kutta scheme for the convective terms. The second-order central difference is used for all the terms in a staggered grid system. The dynamic subgrid scale model (Lilly 1992) is used for LES.

To find an intermediate velocity field $\hat{u}^k_{i,H}$ which provides reduced error in the pressure field, the following correction to $\hat{u}^k_i$ is considered:

$$\hat{u}^k_{i,H} = \hat{u}^k_i - (\gamma_k+\rho_k)\Delta t\left(\frac{\partial}{\partial x_i}\right)_H f,$$

where f is a potential field determining the amount of correction and the subscript H denotes a formal finite volume discrete operator. The expression for f is given as:

$$\begin{aligned}\left(\frac{\partial^2}{\partial x_j \partial x_j}\right)_H f = \left(\frac{\partial^2}{\partial x_j \partial x_j}\right)_H p^{k-1} + \frac{1}{(\gamma_k+\rho_k)}\left[\gamma_k\left(\frac{\partial}{\partial x_i}\frac{\partial}{\partial x_j}\right)_H (u_i u_j)^{k-1}\right. \\ \left. +\rho_k\left(\frac{\partial}{\partial x_i}\frac{\partial}{\partial x_j}\right)_H (u_i u_j)^{k-2}\right] + \frac{1}{(\gamma_k+\rho_k)\Delta t}\left(\frac{\partial}{\partial x_i}\right)_H \hat{u}^k_i.\end{aligned}$$

The grid topology around the CD profile is similar to the LB grid and the same boundary conditions are imposed. A first cartesian grid, termed *Grid1* and shown in

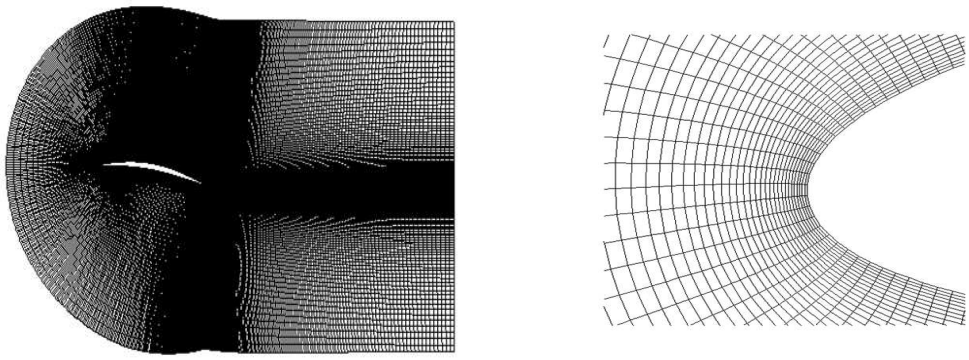

FIGURE 3. Left: Full grid around the CD airfoil used for the DES method. Right: Close-up at the leading edge.

Figure 2 (left), had some local grid stretching which limits the number of points in a two-dimensional slice to 150,000 nodes shown in Figure 2 (left). To avoid numerical problems at the leading edge, the grid spacing is locally uniform as shown in Figure 2 (right). The smallest grid cell at the leading edge is still 2.5 times larger than the one on the body-fitted LES grid. Adding 32 nodes in the spanwise direction, extending over 5% of the chord length, led to a 4.8 millions grid in 3D.

3. Detached-eddy simulation

Spalart *et al.* (1997) proposed a hybrid technique known as detached eddy simulations (DES), which combines URANS and LES models by non-zonal blending. Near the wall a standard RANS model is used and in the outer region of the boundary layer where large detached turbulent structures occur, the URANS equations are modified such that they take a LES-like form. The switching is achieved by modifying the length scale l_{turb} of the turbulence model according to the local grid dimension $\Delta = max\,(\Delta_x, \Delta_y, \Delta_z)$: $\tilde{l} = min\,(l_{turb}, C_{DES}\,\Delta)$. The present simulations obtained with Fluent 6.1.22 are based on the modification of the Spalart-Allmaras transport equation for the modified turbulent kinetic viscosity $\tilde{\nu}$:

$$\frac{\partial \tilde{\nu}}{\partial t} + u_i \frac{\partial \tilde{\nu}}{\partial x_i} = c_{b1}\tilde{S}\tilde{\nu} - c_{w1} f_w \left[\frac{\tilde{\nu}}{\tilde{l}}\right]^2 + \frac{1}{\sigma}\frac{\partial}{\partial x_j}\left[(\nu + \tilde{\nu})\frac{\partial \tilde{\nu}}{\partial x_j}\right] + \frac{c_{b2}}{\sigma}\left(\frac{\partial \tilde{\nu}}{\partial x_j}\right)^2 \qquad (3.1)$$

The value for C_{DES} of 0.65 is based on the validation of the model for decaying isotropic turbulence. This scheme is far less expensive than LES but is suppposed to capture the large scale motions in regions with significant eddy content. Recent applications of the DES to aeroacoustic experiments have yielded promising results: Mendonça, Allen & de Charentenay (2003) have investigated the acoustics of several cavities with the DES method; Greschner *et al.* (2004) have applied the DES method to the complex flow past a rod-airfoil configuration. In the latter, a good agreement was found with the experimental velocity spectra up to 2000 Hz, which corresponds to the frequency range over which significant sound is generated.

Two three-dimensional grids have been built from the original LES grids to yield reduced models that could be run on single-processor 32-bits PC workstations. The first one, termed *DES-Grid1*, stems from the LES grid in a two-dimensional slice but has a

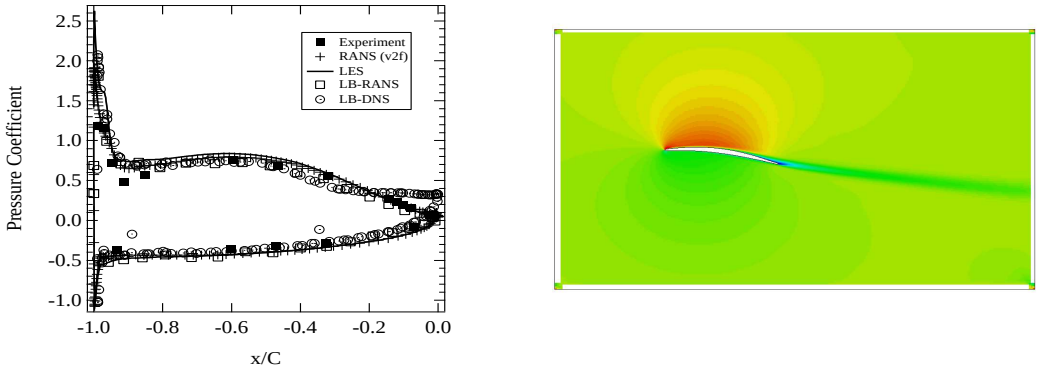

FIGURE 4. Left: Pressure coefficient -C_p. Right: LB-RANS velocity contours.

reduced spanwise extent of 5% of the chord length with 16 equidistant points (Figure 3). The total size of the grid is then ($960 \times 84 \times 16$) and has therefore 1.3 million nodes. A second grid, termed *DES-Grid2*, keeps the original span 10% of the chord length of the reference LES. Yet to limit the overall grid size, two levels of coarsening are applied away from the profile (Figure 5b).

4. Simulation results

The LB method was first run in a URANS mode with a time step of 2.4×10^{-7} s. The DNS mode was later switched on with a time step of 1.9×10^{-7} s. To speed up the computation, the Mach number has been increased from 0.04 to 0.2. Figure 4 (left) shows a comparison of the pressure coefficient of these LB simulations with the corresponding ones from the body fitted RANS performed with Fluent by Moreau *et al.* (2003) and the reference LES simulation by Wang *et al.* (2004). The agreement of the LB-RANS simulation with the other methods is very good even though some oscillations are present, which are even more pronounced in the friction coefficient. Figure 4 (right) is the corresponding flow field, which again matches closely the previous RANS simulation. No unsteadiness is found as in the body fitted RANS results: neither pressure fluctuations along the blade, nor vortical structures in the wake. Results have been gathered for 11 non-dimensional flow-through times based on the chord and free-stream velocity. Switching off the turbulence model and refining the grid produces the so-called LB-DNS results. The refined grid is shown in Figure 5c. The DNS simulation has been run for 6.7 flow-through times. Pressure fluctuations are now produced. Yet, more oscillations on the mean pressure coefficient than in the RANS mode are also obtained. These larger wiggles are apparently generated by the stairstep-like boundary representation and, possibly, the grid refinement. These have been filtered out in Figure 4. The leading edge region is similar. Yet at the trailing edge, the larger adverse pressure gradient triggers a turbulent flow separation not evidenced in the experiment. This is also clearly shown by the darker zones in the streamwise velocity contours (Figures 6c and 7c). The boundary layer is consequently thicker at the trailing edge. This flow separation may have been triggered by a too rapid grid refinement in the aft region of the profile, in the streamwise direction. Finally, the wake exhibits a clear vortex shedding not seen in the reference LES. This is most likely caused by the limited spanwise extent of the grid: achieving the proper

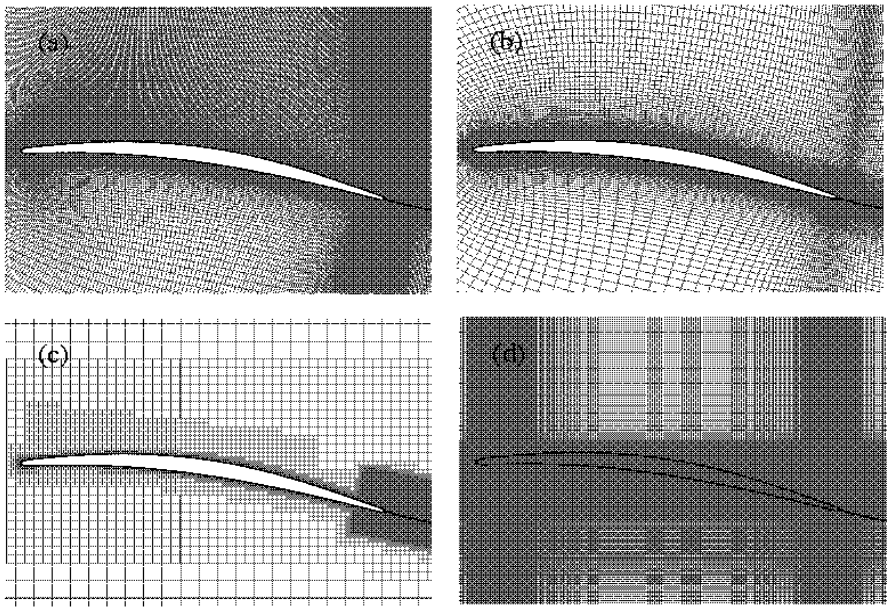

FIGURE 5. Final grids: a) LES, b) DES, c) LB, d) LES-IB.

grid resolution in this direction would require prohibitively expensive three-dimensional simulations.

With the LES-IB method, a first simulation was run at a Reynolds number of 1.5×10^4 on the grid *IB-Grid1*. The Immersed Boundary method yielded a complex three-dimensional laminar wake behind the airfoil. Primary roll-up vortices and secondary rib vortices are found, which are typical structures of three-dimensional vortex shedding. When switching to the actual Reynolds number of 1.5×10^5, numerical instabilities occurred close to the trailing edge and in the wake where the grid stretching is the largest. This motivated switching to the more uniform and finer grid termed *IB-Grid2*. This final grid is shown in Figure 5d. The time step is 1.5×10^{-5} s. The simulation has been run for 5 non-dimensional time after the transient period. At the leading edge, Figure 9 (left) shows a similar pressure plateau as in the reference LES, evidence of a small laminar flow separation. The agreement with experiment is also excellent on both suction and pressure sides. This small recirculation bubble oscillates and triggers small vortices that are then convected along the profile. At the trailing edge, the large vortex shedding shown at the lower Reynolds Number of 1.5×10^4 is no longer observed. Smaller turbulent structures are convected in the wake as shown in the close-up view of both streamwise and spanwise velocity contours at the trailing edge (Figures 7d and 8d). At the trailing edge, the structures are now different from the reference body-fitted simulation. Figure 6 also suggests that the boundary layer is locally thicker. In the aft portion of the profile, the grid spacing is most likely still too large (two to three times larger in the streamwise direction and ten times larger in the wall-normal direction than in the reference body-fitted LES).

The DES simulations have first been run on the shorter grid *DES-Grid1*. The reduced time step selected is 0.025 or a physical time step of about 2×10^{-4} s. This is about one order of magnitude larger than that for the LES simulations. The total simulation

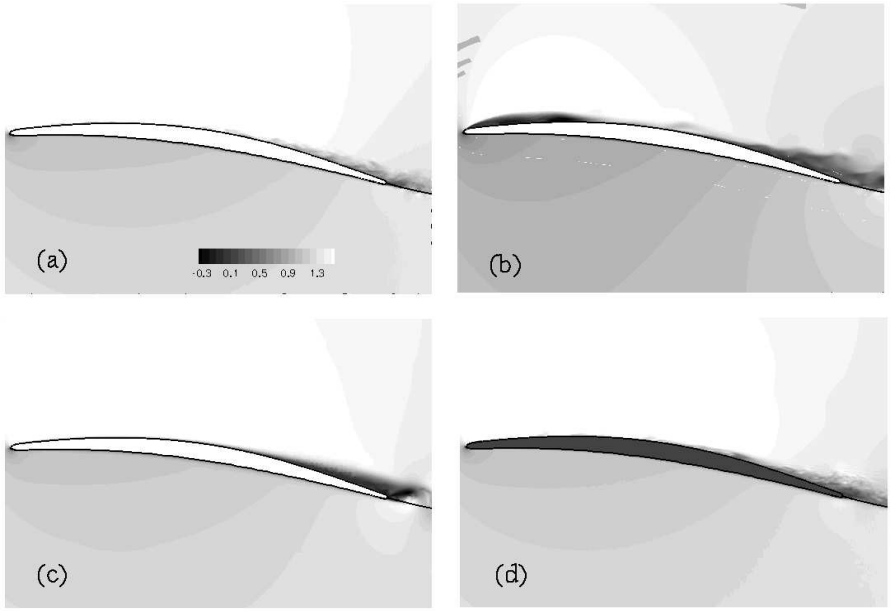

FIGURE 6. Streamwise velocity: a) LES, b) DES, c) LB, d) LES-IB.

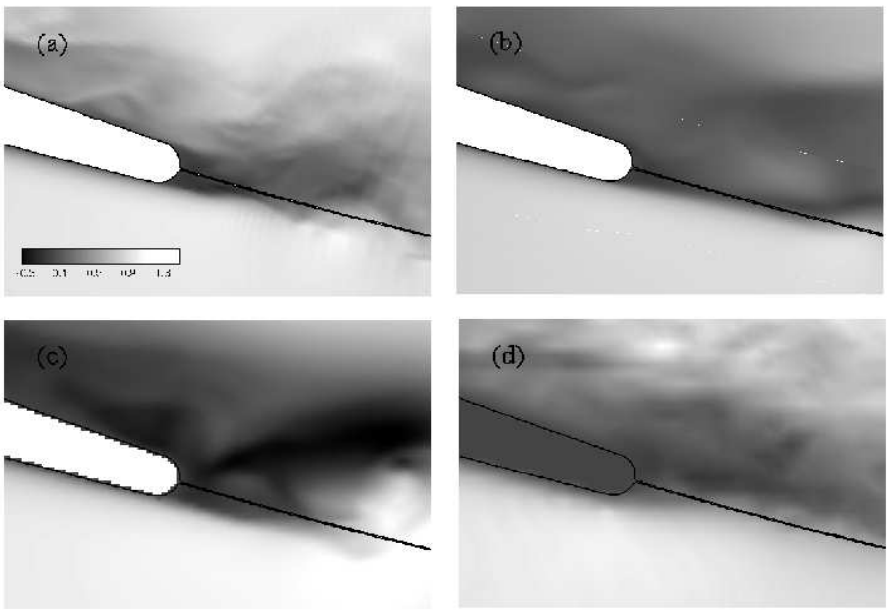

FIGURE 7. Close-up view of streamwise velocity: a) LES, b) DES, c) LB, d) LES-IB.

involved about 800 time steps in 24 hours or 20 flow-through times. Figure 9 (left) shows the corresponding wall pressure distribution. A too-large flow separation at the leading edge is generated yielding the large pressure plateau. The pressure recovery at the trailing edge is however in good agreement with experiment and the other LES simulations. Figure 9 (right), representing an iso-surface of vorticity, clearly shows some

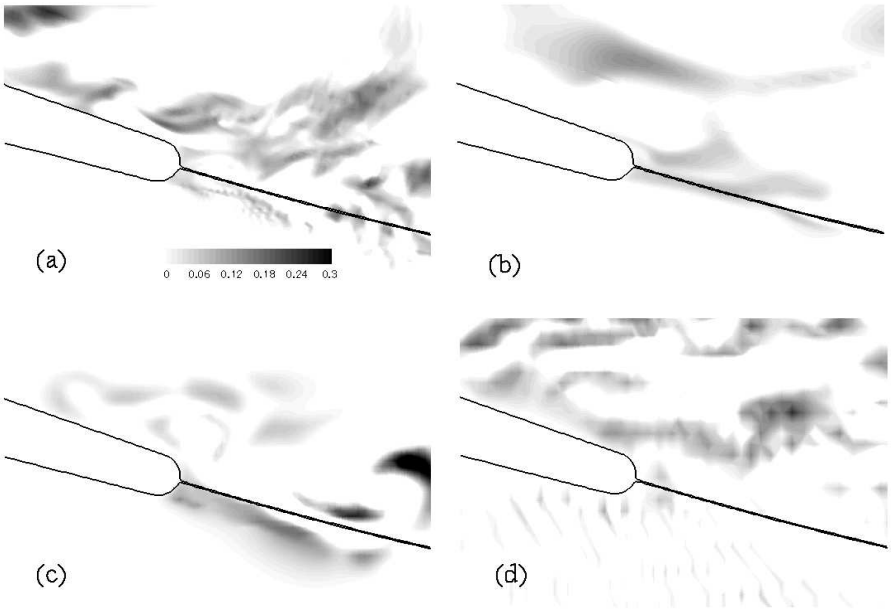

FIGURE 8. Close-up view of spanwise velocity: a) LES, b) DES, c) LB, d) LES-IB.

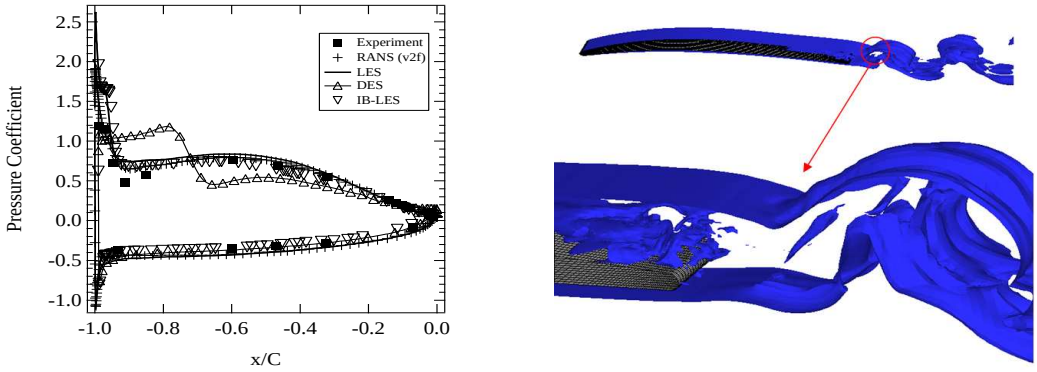

FIGURE 9. Left: Pressure coefficient -C_p. Right: DES iso-surface of vorticity magnitude.

three-dimensional unsteadiness produced close to the trailing edge. Smaller scales are created besides large scale vortex shedding and pressure fluctuations are produced close to the trailing edge. The main structures are much larger than in the LES and exhibit a definite large scale vortex shedding as in the LBM case. This has motivated an extension of the spanwise domain size to yield the grid *DES-Grid2* shown in Figure 5b. Figure 6b represents the streamwise velocity which still exhibits the vortex shedding pattern, but the domain extension has clearly reduced it. The boundary layer thickness is still the largest, which then leads to the widest wake shown in Figure 10.

In this plot, all simulations exhibit a larger wake thickness and a larger velocity deficit both at $x/C = 0.1$ and $x/C = 0.2$ (the trailing edge is located at $x/C = 0$), which suggests a thinner suction side boundary layer at the trailing edge in the experiment. The velocity profile of the reference LES is the closest to the experimental one. The

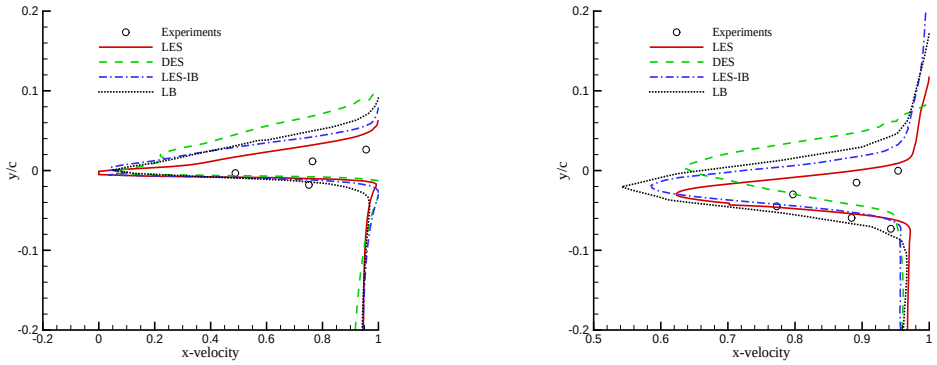

FIGURE 10. Wake Velocity Profiles. Left: $x/C = 0.1$. Right: $x/C = 0.2$.

LES-IB profile is thicker but its spreading is the same. This can again be attributed to the lower grid resolution compared to the reference LES. The LB-DNS profile is only slightly thicker at the first station but it spreads faster and the wake thickness is now wider on both suction and pressure sides. This might be due to a local grid discontinuity. The DES profile at the first station has the same thickness on the pressure side as the experiment and the other methods. On the suction side, however, it first follows the two LES profiles and then becomes suddenly larger, because of the observed larger structures. The switch in the model might be the cause of this sudden jump in the velocity profile. Downstream, at the second station, the wake thickness is similar to the LB-DNS one and the wake spreading is similar to the experiment. Yet the profile is shifted, suggesting a wake that is almost straight, which should not be the case due to the lift of the cambered CD airfoil. Finally, it should be stressed that the experimental grid for the X-wire probe is probably not fine enough to capture the minimum velocity and that the measurement at this location also carries the largest measurement uncertainty in this region.

To compare the pressure fluctuations obtained by all methods, the wall pressure power spectral density (PSD) has been computed at the sensor closest to the trailing edge, located at $x/C = -0.02$ on the suction side. These PSDs are compared in Figure 11. The reference LES provides a very good agreement with the fluctuations measured by the remote microphone probe. All other simulations yield much higher spectral levels at low frequencies. These overpredictions of lower frequency fluctuations and faster decay at higher frequencies may be partly attributable to the lower grid resolution in the trailing edge region for the LB-DNS and LES-IB methods. Other issues, such as the boundary treatment in LES-IB and the lack of a SGS model in LB-DNS also need to be examined. In the DES, the same grid is used in the inner region as in the reference LES, which might explain the good agreement at high frequencies. Yet the large unphysical flow structures cause an overprediction in the low and intermediate frequency range of the spectrum. The LB-DNS exhibits a broad peak around 350 Hz which can be attributed to the wake vortex shedding seen in the simulation. The lack of small structures in this simulation causes the faster decay of LB-DNS spectrum at high frequencies. By examining the pressure traces, some transients are found to be still present in the DES and LB simulations, which suggests that the solutions have not fully settled down to a statistically steady state, or that some pressure reflections (numerical noise) might be present at the boundaries.

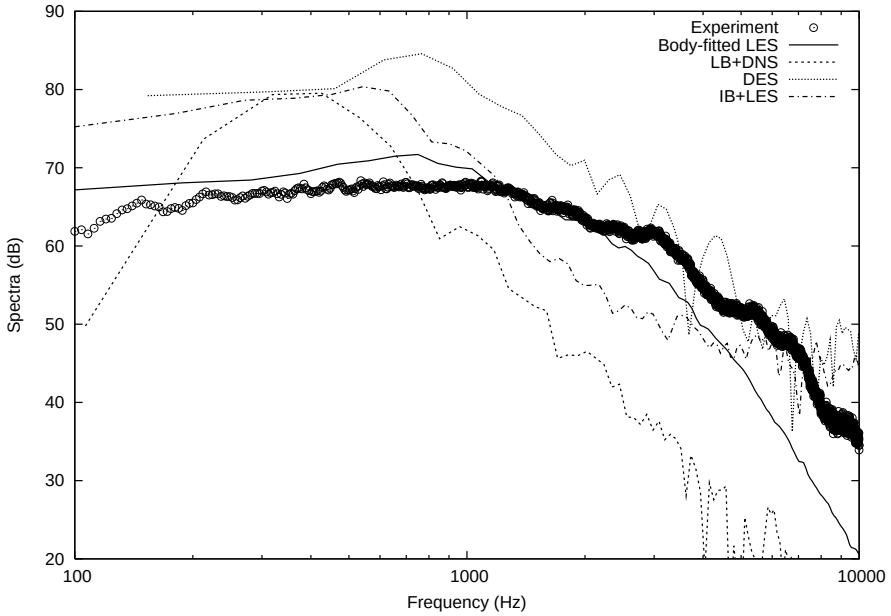

FIGURE 11. Power spectral density of wall pressure near the trailing edge ($x/C = -0.02$ on suction side): a) LES, b) DES, c) LB, d) LES-IB.

5. Conclusions

The ability to perform LES with an immersed boundary method at high Reynolds number has been demonstrated. The current simulation has provided good resolution of the small structures developing along the airfoil and a proper mean wall pressure distribution. The grid resolution is still too coarse in the trailing edge area, which may have caused the less favorable wall pressure spectra and wider velocity profile in the wake. Moreover, the grid requirements of a single block structured cartesian grid are as restrictive as the body-fitted approach. A lot of grid nodes have to be clustered in the airfoil region and a very regular, quasi-uniform grid distribution has to be used to prevent numerical unstability or numerical wiggles in the solution. A possible solution is to use local grid refinement as shown by Mittal & Iaccarino (2005). The effect of the immersed boundary treatment on the wall pressure spectra also needs to be investigated.

The LBM is clearly not suited for this type of simulation yet. The grid requirements are similar to those of the IB method in the streamwise and wall-normal directions. The local grid refinement capability clearly helps reduce the number of surfels in the profile plane. However too rapid grid refinements in the trailing edge region produce a flow separation not seeen experimentally. Moreover, the restriction to cubic voxels does not allow a sufficent extension of the three-dimensional grid in the spanwise direction, which prevents the proper streching of the vortical structures in the wake. In fact, all simulations on grids that have a limited spanwise extent have triggered unphysical two-dimensional vortex shedding. At least a spanwise extension of 10% of the chord length is required. The current grid topology of Powerflow is the main limitation of this LBM implementation. It should also be remembered that the LB simulation is an under-resolved DNS, making it difficult to compare the results with other LES solutions.

The DES does not provide a physical flow topology even on the fine reference LES

grid, with too large a flow separation at the leading edge and too large flow structures and too thick a boundary layer at the trailing edge. The numerical treatment of the inlet boundary condition in Fluent 6.1.22 may not be sufficient to prevent some wave reflection and random noise generation that consequently modify the wall pressure fluctuations.

In summary, none of the methods tested here can yet provide a satisfactory alternative to the body-fitted LES to tackle the larger and more complex three-dimensional flow over a fan blade with its complex tip clearance labyrinth.

REFERENCES

Caro, S. & Moreau, S. 2000 Aeroacoustic modeling of low pressure axial flow fans. *AIAA Paper 2000-2094*, 6^{th} AIAA/CEAS Aeroacoustics Conference, Lahaina, Hawaii.

Chen, S., Teixeira, C. & Molvig, K. 1997 Digital physics approach to computational fluid dynamics: some basic theoretical features. *Int. J. Modern Phy. C* **8**, 675-684.

Chen, S. & Doolen, D. 1998 Lattice Boltzmann method for fluid flows. *Annu. Rev. Fluid Mech.* **30**, 329-364.

Chen, S., Kandasamy, S., Orszag, S., Shock, R., Succi, S. & Yakhot, V. 2003 Extended Boltzmann kinetic equation for turbulent flows. *Science* **301**, 633-636.

Fadlun, E. A., Verzicco, R., Orlandi, P. & Mohd-Yusof, J. 2000 Combined immersed-boundary/finite-difference methods for three-dimensional complex flow simulations. *J. Comput. Phys.* **161**, 35-59.

Fukano, T., Kodama, Y. & Senoo, Y. 1977 Noise generated by low pressure axial flow fans. 1 - Modelling of the turbulent noise. *J. Sound Vib.* **50**, 63-74.

Glegg, S. A. L., Baxter, S. M. & Glendinning, A. G. 1987 The prediction of broadband noise from wind turbines. *J. Sound Vib.* **118**, 217-239.

Greschner, B., Thiele, F., Casalino, D. & Jacob, M. C. 2004 Influence of turbulence modeling on the broadband noise simulation of complex flows. *AIAA Paper 2004-2926*, 10^{th} AIAA/CEAS Aeroacoustics Conference, Manchester, United Kingdom.

Hubbard, H. H. & Shepherd, K. P. 1991 Aeroacoustics of large wind turbines. *J. Acoust. Soc. Am.* **89**, 2495-2507.

Kim, J. & Moin, P. 1985 Application of a fractional-step method to incompressible Navier-Stokes equations. *J. Comput. Phys.* **59**, 308-323.

Lilly, D. K. 1992 A proposed modification of the Germano subgrid-scale closure method. *Phys. Fluids A* **4**, 633-635.

Mendonça, F., Allen, R. & de Charentenay, J. 2003 CFD prediction of narrowband and broadband cavity acoustics at $M = 0.85$. *AIAA Paper 2003-3303*, 9^{th} AIAA/CEAS Aeroacoustics Conference, Hilton Head, South Carolina.

Mittal, M. & Iaccarino, G. 2005 Immersed boundary methods. To be published in *Annu. Rev. Fluid Mech.*

Moreau, S., Henner, M., Iaccarino, G., Wang, M. & Roger, M. 2003 Analysis of flow conditions in free-jet experiments for studying airfoil self-noise. *AIAA J.* **41**, 1895-1905.

Parchen, R., Hoffmans, R., Gordner, A., Braun, K. A., van der Borg, N. J. C. & Dassen, M. and A.G.M. 1999 Reduction of airfoil self-noise at low Mach

number with a serrated trailing edge. 6^{th} International Congress on Sound and Vibration, Copenhagen, Denmark, pp. 3433-3440.

PÉRENNÈS, S. & ROGER, M. 1998 Aerodynamic noise of a two-dimensional wing with high-lift devices. *AIAA Paper 98-2338*, 4^{th} AIAA/CEAS Aeroacoustics Conference, Toulouse, France.

ROGER, M. & MOREAU, S. 2004 Trailing edge noise measurements and prediction for a subsonic loaded fan blade. *AIAA J.* **42**, 536-544.

SHARLAND, I. J. 1964 Sources of noise in axial flow fans. *J. Sound Vib.* **1**, 302-322.

SINGER, B. A., LOCKARD, D. P. & BRENTNER, K. S. 2000 Computational aeroacoustic analysis of slat trailing-edge flow. *AIAA J.* **38**, 1558-1564.

SPALART, P. R., JOU, W. H., STRELETS. M. & ALLMARAS. S. R. 1997 Comments on the feasibility of LES for wings and a hybrid RANS/LES approach. 1^{st} AFSOR International Conference on DNS/LES, Aug. 4-8; see also: *Advances in DNS/LES.* C. Liu and Z. Liu Eds, Greyden Press, Columbus, OH.

WANG, M., MOREAU, S., IACCARINO, G. & ROGER, M. 2004 LES prediction of wall pressure spectra on a low speed airfoil. *Annual Research Briefs-2004*, Center for Turbulence Research, Stanford Univ./NASA Ames.

WRIGHT, S.E. 1976 The acoustic spectrum of axial flow machines. *J. Sound Vib.* **45**, 165-223.

YOU, D., MITTAL, M., WANG, M. & MOIN, P. 2004 Computational methodology for large-eddy simulation of tip-clearance flows. *AIAA J.* **42**, 271-279.